94 β-Decay Half-Lives of Neutron-Rich $_{55}$Cs to $_{67}$Ho: Experimental Feedback and Evaluation of the *r*-Process Rare-Earth Peak Formation

J. Wu,[1,2,*] S. Nishimura,[2] G. Lorusso,[2,3,4] P. Möller,[5] E. Ideguchi,[6] P.-H. Regan,[3,4] G. S. Simpson,[7,8,9] P.-A. Söderström,[2] P. M. Walker,[4] H. Watanabe,[10,2] Z. Y. Xu,[11,12] H. Baba,[2] F. Browne,[13,2] R. Daido,[14] P. Doornenbal,[2] Y. F. Fang,[14] N. Fukuda,[2] G. Gey,[7,15,2] T. Isobe,[2] Z. Korkulu,[16] P. S. Lee,[17] J. J. Liu,[11] Z. Li,[1] Z. Patel,[4,2] V. Phong,[18,2] S. Rice,[4,2] H. Sakurai,[2,12] L. Sinclair,[19,2] T. Sumikama,[2] M. Tanaka,[6] A. Yagi,[14] Y. L. Ye,[1] R. Yokoyama,[20] G. X. Zhang,[10] D. S. Ahn,[2] T. Alharbi,[21] N. Aoi,[6] F. L. Bello Garrote,[22] G. Benzoni,[23] A. M. Bruce,[13] R. J. Carroll,[4] K. Y. Chae,[24] Z. Dombradi,[16] A. Estrade,[25] A. Gottardo,[26,27] C. J. Griffin,[25] N. Inabe,[2] D. Kameda,[2] H. Kanaoka,[14] I. Kojouharov,[28] F. G. Kondev,[29] T. Kubo,[2] S. Kubono,[2] N. Kurz,[28] I. Kuti,[16] S. Lalkovski,[4] G. J. Lane,[30] E. J. Lee,[24] T. Lokotko,[11] G. Lotay,[4] C.-B. Moon,[31] D. Murai,[2] H. Nishibata,[14] I. Nishizuka,[32] C. R. Nita,[13] A. Odahara,[14] Zs. Podolyák,[4] O. J. Roberts,[33] H. Schaffner,[28] C. Shand,[4] Y. Shimizu,[2] H. Suzuki,[2] H. Takeda,[2] J. Taprogge,[34,35] S. Terashima,[10] Z. Vajta,[16] and S. Yoshida[14]

[1]*School of Physics and State Key Laboratory of Nuclear Physics and Technology, Peking University, Beijing 100871, China*
[2]*RIKEN Nishina Center, 2-1 Hirosawa, Wako-shi, Saitama 351-0198, Japan*
[3]*National Physical Laboratory, NPL, Teddington, Middlesex TW11 0LW, United Kingdom*
[4]*Department of Physics, University of Surrey, Guildford GU2 7XH, United Kingdom*
[5]*Theoretical Division, Los Alamos National Laboratory, Los Alamos, New Mexico 87545, USA*
[6]*Research Center for Nuclear Physics (RCNP), Osaka University, Ibaraki, Osaka 567-0047, Japan*
[7]*LPSC, Universite Joseph Fourier Grenoble 1, CNRS/IN2P3, Institut National Polytechnique de Grenoble, F-38026 Grenoble Cedex, France*
[8]*School of Engineering, University of the West of Scotland, Paisley, PA1 2BE, United Kingdom*
[9]*Scottish Universities Physics Alliance, University of Glasgow, Glasgow, G12 8QQ, United Kingdom*
[10]*IRCNPC, School of Physics and Nuclear Energy Engineering, Beihang University, Beijing 100191, China*
[11]*Department of Physics, the University of Hong Kong, Pokfulam Road, Hong Kong*
[12]*Department of Physics, University of Tokyo, Hongo 7-3-1, Bunkyo-ku, 113-0033 Tokyo, Japan*
[13]*School of Computing Engineering and Mathematics, University of Brighton, Brighton, BN2 4GJ, United Kingdom*
[14]*Department of Physics, Osaka University, Machikaneyama-machi 1-1, Osaka 560-0043 Toyonaka, Japan*
[15]*Institut Laue-Langevin, B.P. 156, F-38042 Grenoble Cedex 9, France*
[16]*Institute for Nuclear Research, Hungarian Academy of Sciences, P. O. Box 51, Debrecen, H-4001, Hungary*
[17]*Department of Physics, Chung-Ang University, Seoul 156-756, Republic of Korea*
[18]*Faculty of Physics, VNU Hanoi University of Science, 334 Nguyen Trai, Thanh Xuan, Hanoi, Vietnam*
[19]*Department of Physics, University of York, Heslington, York, YO10 5DD, United Kingdom*
[20]*Center for Nuclear Study (CNS), University of Tokyo, Wako-shi, Saitama 351-0198, Japan*
[21]*Department of Physics, College of Science in Zulfi, Almajmaah University, P.O. Box 1712, 11932, Saudi Arabia*
[22]*University of Oslo, P.O. Box 1072 Blindern, 0316 Oslo, Norway*
[23]*INFN, Sezione di Milano, via Celoria 16, I-20133 Milano, Italy*
[24]*Department of Physics, Sungkyunkwan University, Suwon 440-746, Republic of Korea*
[25]*School of Physics and Astronomy, University of Edinburgh, Edinburgh EH9 3JZ, United Kingdom*
[26]*Dipartimento di Fisica dellUniversit' degli Studi di Padova, I-35131 Padova, Italy*
[27]*INFN, Laboratori Nazionali di Legnaro, Legnaro I-35020, Italy*
[28]*GSI Helmholtzzentrum für Schwerionenforschung GmbH, 64291 Darmstadt, Germany*
[29]*Nuclear Engineering Division, Argonne National Laboratory, Argonne, Illinois 60439, USA*
[30]*Department of Nuclear Physics, R.S.P.E., Australian National University, Canberra, A.C.T. 0200, Australia*
[31]*Hoseo University, Asan, Chungnam 336-795, Korea*
[32]*Department of Physics, Tohoku University, Aoba, Sendai, Miyagi 980-8578, Japan*
[33]*School of Physics, University College Dublin, Belfield, Dublin 4, Ireland*
[34]*Departamento de Física Teórica, Universidad Autónoma de Madrid, E-28049 Madrid, Spain*
[35]*Instituto de Estructura de la Materia, CSIC, E-28006 Madrid, Spain*

The β-decay half-lives of 94 neutron-rich nuclei $^{144-151}$Cs, $^{146-154}$Ba, $^{148-156}$La, $^{150-158}$Ce, $^{153-160}$Pr, $^{156-162}$Nd, $^{159-163}$Pm, $^{160-166}$Sm, $^{161-168}$Eu, $^{165-170}$Gd, $^{166-172}$Tb, $^{169-173}$Dy, $^{172-175}$Ho, and two isomeric states ^{174m}Er, ^{172m}Dy were measured at the Radioactive Isotope Beam Factory, providing a new experimental basis to test theoretical models. Strikingly large drops of β-decay half-lives are observed

at neutron-number $N = 97$ for $_{58}$Ce, $_{59}$Pr, $_{60}$Nd, and $_{62}$Sm, and $N = 105$ for $_{63}$Eu, $_{64}$Gd, $_{65}$Tb, and $_{66}$Dy. Features in the data mirror the interplay between pairing effects and microscopic structure. *r*-process network calculations performed for a range of mass models and astrophysical conditions show that the 57 half-lives measured for the first time play an important role in shaping the abundance pattern of rare-earth elements in the solar system.

The rapid neutron-capture (*r*-) process, a series of neutron captures competing with β decays occurring in extreme neutron-rich stellar environments, is responsible for the origin of about half of the elements heavier than iron in the Universe [1]. The fact that the astrophysical sites of the *r* process and its exact mechanism have not been identified yet makes the *r* process one of the most exciting subjects in astrophysics [2].

The two most prominent features of the *r*-process abundance in the solar system are the large abundance of $_{52}$Te, $_{54}$Xe (mass number $A \sim 130$) and $_{78}$Pt, $_{79}$Au ($A \sim 195$), which are understood in terms of the enhanced stability of nuclei with filled major neutron shells (of neutron number $N = 82$ and $N = 126$). However, the production mechanism of the smaller and broader peak of rare-earth elements (REE) ($A \sim 165$) is instead still a controversial topic [3–5]. In environments with extremely high neutron-to-seed ratios, such as in merging neutron stars, the *r* process may synthesize very heavy nuclei ($A > 278$), which then decay by nuclear fission. The REE peak could receive a major contribution from such a process and its structure could reflect closely the mass distribution of fission fragments [6,7]. Alternatively, the REE peak could be formed in any astrophysical sites where a long duration $(n,\gamma) \rightleftharpoons (\gamma,n)$ equilibrium persisted, during the *r*-process freeze-out when the temperature or neutron density are too low to sustain the explosive nuclear burning. The signature of this dynamical formation mechanism would be encoded in masses (as well as β-decay and neutron-capture rates) [4]. The currently unknown nuclear structure of exotic nuclei could be embodied in the REE peak. In this region of the nuclear chart, *K* mixing, vibration degeneracy, shape coexistence, quadrupole deformation, and the strength of the first-forbidden β decays are highly uncertain. Shell gaps arising from mid-shell deformation are of special interest for the *r* process, and, recently, evidence for a deformed shell gap was reported in $_{64}$Gd and $_{62}$Sm at $N = 100$ [8].

Therefore, the REE peak may contain a unique signature of the unknown astrophysical sites, possibly of the late *r*-process conditions to which the main *r*-process peaks may be insensitive [9]. However, to interpret such a signature, the various nuclear processes such as fission, neutron capture, and β-decay of exotic nuclei have to be experimentally known or reliably modeled. This Letter reports on the first measurements of a large set of β-decay half-lives and their systematic trends, whose theoretical predictions are difficult because the half-lives depend on a multitude of nuclear properties, for example, deformation, level structure and spin, as well as Q_β.

Two β-decay spectroscopy experiments optimized for transmission of ^{158}Nd and ^{170}Dy were performed at the Radioactive Isotope Beam Factory (RIBF) by using in-flight fission of a 345 MeV/A ^{238}U primary beam with an average intensity of 7 and 12 pnA, respectively. After selection and identification in the large-acceptance BigRIPS separator, exotic nuclei of interest were transported through the ZeroDegree Spectrometer (ZDS) and implanted in the beta-counting system Wide range Active Silicon-Strip Stopper Array for Beta and ion detection (WAS3ABi) at a rate of about 100 ions/s [10]. High purity germanium cluster detectors of the Euroball RIken Cluster Array (EURICA) surrounded WAS3ABi to detect any γ rays emitted from the implanted nuclei [11–18]. The particle identification (PID) achieved with the TOF-Bρ-ΔE method is shown in a two-dimensional plot of atomic number (*Z*)

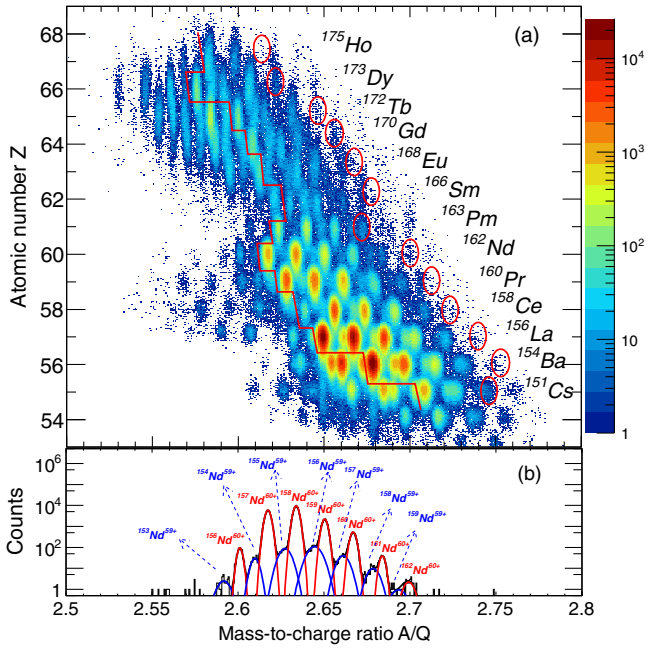

FIG. 1. (a) Particle identification plot. The nuclides with newly measured β-decay half-lives are located to the right of the red line, and the nuclei tagged by red circles are the most exotic isotopes measured for each element. (b) The A/Q distribution for the case of $_{60}$Nd isotopes.

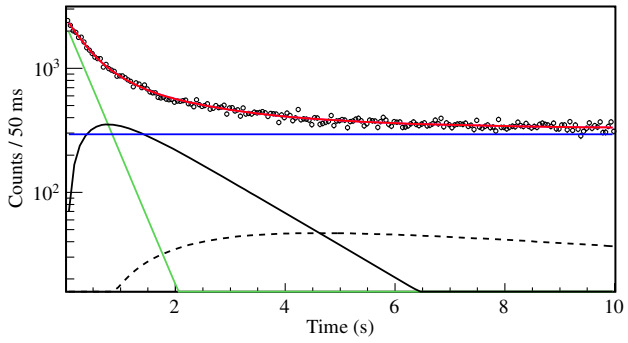

FIG. 2. Time distribution of ^{157}Pr β-decay events fitted to the sum of activities of several components: parent nuclei (solid green line), daughter nuclei (solid black line), granddaughter nuclei (dashed black line), as well as a constant background (solid blue line). The other components, including β-delayed daughter nuclei and β-delayed granddaughter nuclei, are not shown in this figure.

versus mass-to-charge ratio (A/Q) [19] (see Fig. 1). The largest source of contamination in our PID was caused by electron pickup of fully stripped ions, a process that alters the A/Q ratios of the ions. However, as shown in Fig. 1, the BigRIPS resolution was high enough to allow identification of a large fraction of these cases. A/Q gates in the off-line analysis allowed control of the purity of the ions, so that it could be accounted for in the half-life analysis. The β-decay half-life of an isotope of interest was extracted from the fit of the time distribution of electrons detected after the implantation of an ion, and correlated to them in position and time [20–24], employing the least-squared and unbinned maximum likelihood methods in a parallel analysis that included contributions from the decays of parent, daughters, granddaughters, as well as a constant background. In some cases, β-decay curves gated on β-delayed γ rays were used to confirm the previous results. The half-lives of daughter nuclei used in the fit were either measured in our experiment or taken from literature [25]. The β-delayed neutron emission probabilities (P_n) were taken from literature [25] if available. Whereas they were varied in the fit within a range up to $\pm 20\%$, and the mean value was determined from the average of theoretical predictions of finite-range droplet-model (FRDM) mass formula with quasi-particle-random-phase approximation (QRPA) [26] and Koura-Tachibana-Uno-Yamada (KTUY) with the second generation of β-decay gross theory (GT2) [27,28]. The final uncertainty of measured half-lives included the contribution from half-lives of daughter, β-delayed daughters, as well as contaminations. In general, the largest contribution to such uncertainty is either statistics due to low count rates or the unknown P_n values. An example of the decay curve fitted for ^{157}Pr is in Fig. 2.

The measured half-lives are reported in the Table (see Supplemental Material [29]). Figure 3 shows the systematic trends of β-decay half-lives as functions of neutron number N. Experimental results are compared with previous measurements, and the predictions of three theoretical models: FRDM + QRPA [26], KTUY + GT2 [27,28], and the relativistic Hartree-Bogoliubov (RHB) with the proton-neutron relativistic quasiparticle random phase approximation (pn-RQRPA) [30]. Our measurements are in very good agreement with the literature values, while discrepancies with theoretical predictions in some cases reach 1 order of magnitude. These differences, however, are within model uncertainty, as one can infer from that they are of similar magnitude for less exotic cases. Our data show, therefore, no evidence for drastic changes of nuclear structure capable of modifying gross properties such as half-lives. To some extent, given the sensitivity of the β-decay half-life to Q_β ($T_{1/2} \propto Q_\beta^{-5}$), we also conclude that there are no dramatic differences appearing between calculated and experimental nuclear masses in the region of nuclei measured here. The KTUY + GT2 and FRDM + QRPA models both reproduce the systematic trends of odd-even staggering present in the experimental results, while the RHB + pn-RQRPA model does not. Among the three models, the KTUY + GT2 provides the most consistent predictions across all the elements considered. In contrast, FRDM + QRPA underestimates systematically the half-lives of $_{59}$Pr, $_{61}$Pm, and $_{67}$Ho isotopes, and RHB + pn-RQRPA shows systematic differences with respect to experiment, which depend on atomic number Z. In particular, the underestimate of half-lives seen for $_{55}$Cs isotopes slowly evolves with Z to a substantial overestimate for $_{65}$Tb, $_{67}$Ho isotopes. Finally, we observe that KTUY + GT2 does not seems to be able to predict effects due to the fine nuclear structure and the complex nature of the β decay. This is likely a consequence of the phenomenological approach of the GT2 model. For these effects, we find that the FRDM + QRPA model allows a more detailed interpretation of the measured data, as described in the following.

A very interesting feature of the half-lives systematics seen in Fig. 3 is the sudden drops at $N = 97$ for the elements $_{58}$Ce, $_{59}$Pr, $_{60}$Nd, and $_{62}$Sm, and at $N = 105$ for $_{63}$Eu, $_{64}$Gd, $_{65}$Tb, and $_{66}$Dy, but with only small drops from $N = 98$ to $N = 99$ and from $N = 106$ to $N = 107$. It is well known that the nucleon-nucleon pairing interaction causes large fluctuations in Q_β along even-A β-decay chains but has no net effect in odd-A decay chains. For the $_{60}$Nd isotope chain, the effect leads to a Q_β increases by about 2 MeV from ^{156}Nd$_{96}$ to ^{157}Nd$_{97}$ then drops by about 1 MeV in ^{158}Nd$_{98}$, with corresponding large fluctuations in the half-lives (see Fig. 3). The calculated β-decay strength function of ^{157}Nd$_{97}$ shows a stronger low-lying strength than ^{156}Nd$_{96}$, which makes the decrease of half-life of ^{157}Nd$_{97}$ relative to ^{156}Nd$_{96}$ larger than what could be expected from Q_β systematics alone [see Figs. 4(a), 4(b)]. Alternatively, from ^{158}Nd$_{98}$ and ^{159}Nd$_{99}$ the calculated and measured drops are much smaller than the expectation that is simply predicted from Q_β changes. The reason is that the strength in the ^{159}Nd$_{99}$ decay is shifted upward by about 2 MeV relative to ^{158}Nd$_{98}$ with the almost identical

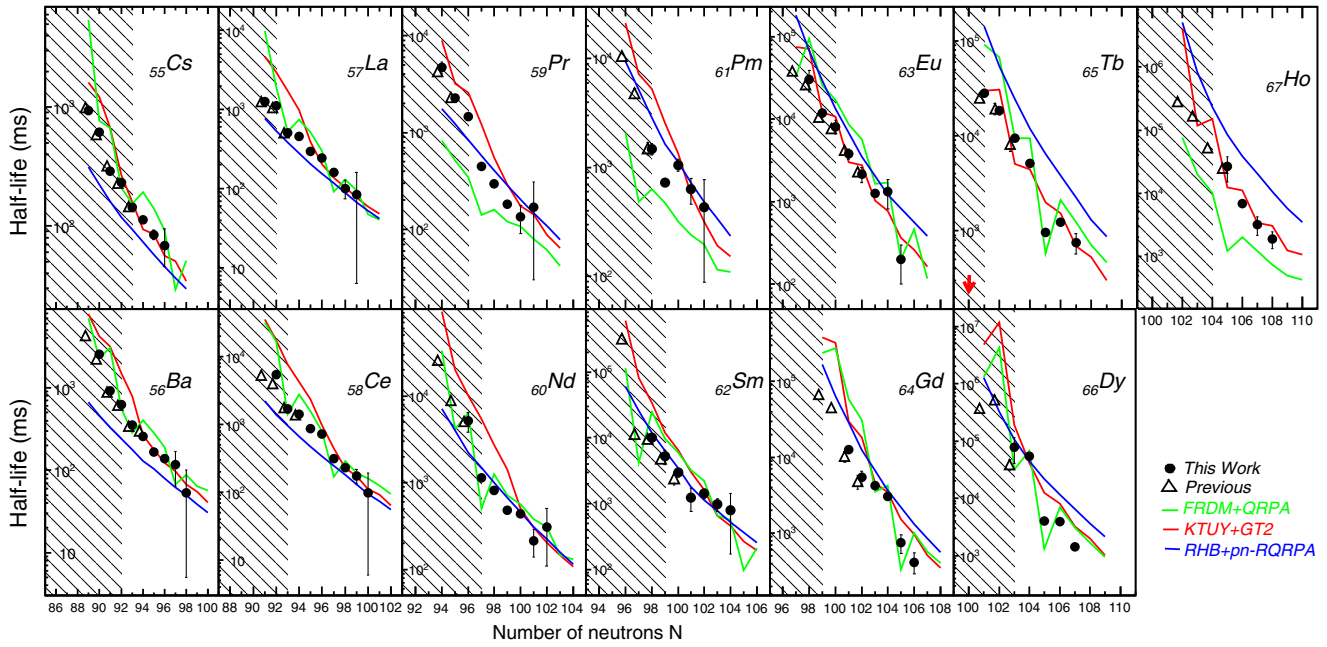

FIG. 3. Systematic trends of β-decay half-lives from this work (solid circles) and previous measurements (open triangles) [25] with neutron number for thirteen elements. The measurements are compared to predictions of three theoretical models: FRDM + QRPA [26] (green), KTUY + GT2 [27,28] (red), and RHB + *pn*-RQRPA [30] (blue). The shaded areas are the currently known-masses region for each element [31], except for the unknown mass of $^{165}_{65}$Tb (red arrow).

distributions below Q_β, canceling the effect of about 2 MeV increase in Q_β [see Figs. 4(c), 4(d)]. Since the ground-state (GS) deformation changes very little along this sequence of isotopes, we can understand these strength-function changes from level spins and GT selection rules. The level schemes here are calculated in the folded-Yukawa model with ground-state deformations [32]. Each level is doubly degenerate. The 31st proton, 49th and 50th neutron levels have the spins of $5/2^-$, $5/2^-$, and $1/2^-$, respectively. For ^{157}Nd$_{97}$ and ^{158}Nd$_{98}$, the neutron in level 49 can decay to the (GS) proton level 31 ($5/2^- \rightarrow 5/2^-$) in the daughter. But the single neutron in level 50 ($1/2^-$) cannot decay to the GS proton level 31 ($5/2^-$) for ^{159}Nd$_{99}$, because the spin difference is 2. Therefore, a (paired) neutron in level 49 decays instead, which leaves 3 unpaired particles in the daughter: one in proton level 31, one in each of neutron levels 49 and 50. Two more unpaired particles than in the GS of ^{159}Pm$_{98}$ leaves it in an about two-MeV excited state. The situation in nuclei near $N = 105$ is similar. Although different spins are involved, the selection rules lead to analogous effects. These effects, which are clear in the data and predicted by the QRPA calculations are not always as easy to disentangle as in the above examples, because additional factors come into play, for example, deformation changes, occupation numbers due to pairing, and wave functions consisting of several asymptotic components.

Concerning the interesting case of $N = 100$, where evidence for a deformed subshell gap was discussed [8], we could not find a convincing signature in the half-life trend. The half-life of $^{161}_{61}$Pm$_{100}$ is longer than that of $^{160}_{61}$Pm$_{99}$, which is somewhat intriguing (see Fig. 3), but similar features were not found in other elements.

To evaluate the impact of the newly measured half-lives on the *r*-process modeling, fully dynamic *r*-process network calculations [33] were performed. As to the role of half-lives in the dynamical REE peak formation we intend to study,

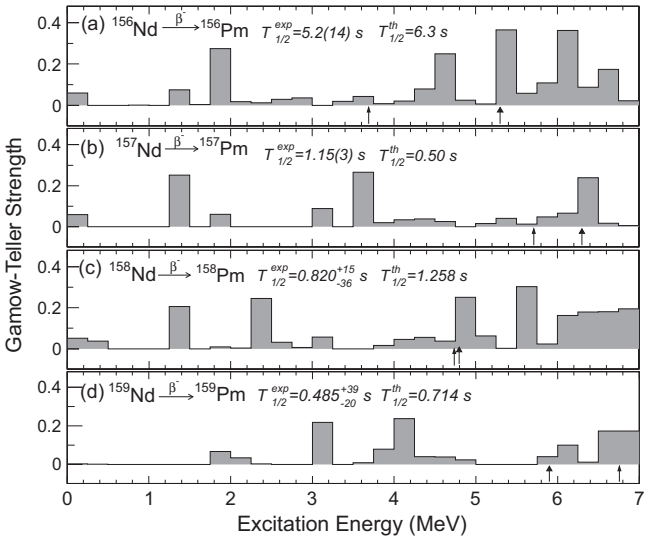

FIG. 4. Gamow-Teller strength functions in the daughter states following β^- decay of the two isotopes $^{156-159}$Nd calculated in the FRDM + QRPA model. The thin vertical arrow indicates the Q_β value, the slightly thicker arrow indicates the neutron-separation energy.

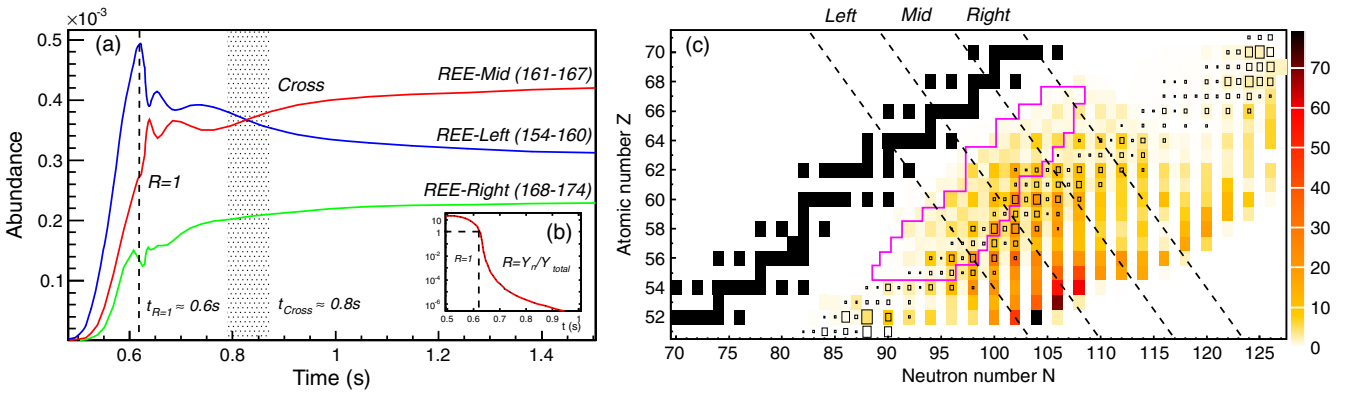

FIG. 5. (a) Time evolution of abundances summed over isobaric chains in the three mass regions $A = 154$–160 (blue), $A = 161$–167 (red), and $A = 168$–174 (green). (b) Time evolution of the ratio (R) between the neutron abundance (Y_n) and the total nuclei abundance ($Y_{\rm total}$). (c) The sensitivity factor $F(Z,N)$ of neutron-rich nuclei with $Z = 52$–70, and the isotopes with the largest abundance at $t \approx 0.8$ s (empty squares). The nuclei measured in this work are the ones within the magenta perimeter. The sensitivity factor is defined therein as $F(Z,N) = 100 \sum_{A=150}^{178} |Y_{\uparrow}(Z,N,A) + Y_{\downarrow}(Z,N,A) - 2Y_{\rm origin}(A)|$ based on Ref. [37]. Where the $Y_{\uparrow}(Z,N,A)$ and $Y_{\downarrow}(Z,N,A)$ are the calculated abundances at mass number A with 10 times and one-tenth of the β-decay half-lives of one specific nuclide (Z,N), respectively. $Y_{\rm origin}(A)$ is the calculated baseline abundance.

where the higher impact from our data is expected, we choose conditions that are typical of the hot r-process not leading to fission recycling. We assumed an initial electron fraction $Y_e = 0.3$ and the entropy $S = 220$ kb/baryon. The time evolution of the temperature after explosion followed an exponential decay with the time constant $\tau = 80$ ms. The matter density followed the same exponential decay but convoluted with a hyperbolic function gradually approaching free expansion [33]. The fine tuning of these conditions was determined by the best reproduction of the REE peak, and does not affect our conclusions as explained in the following. The mass models used in our study were FRDM, KTUY05 [34], HFB-14 (Hartree-Fock-Bogolyubov-14) [35], and all reaction rates for our baseline calculations were taken from the JINA ReaclibV1.0 database [36]. For each mass model we study the effect of our new data to calculations that use half-lives predictions from the three models discussed above (see Fig. 3). The impact of half-lives for each mass model is comparable; therefore in the following we show the result only using KTUY05.

To illustrate the dynamics of the formation of the REE peak in our model, we compare in Fig. 5(a) the time evolution of abundances summed over isobaric chains in the three mass regions $A = 154$–160, $A = 161$–167, and $A = 168$–174. These regions contain the progenitors of the rising, central, and falling wing of the REE peak. As shown in Fig. 5(a), the three summed abundances rise sharply when free neutrons are numerous ($R = Y_n/Y_{\rm total} > 1$), and change slowly later during freeze-out. A large decrease of the abundance in the mass region $A = 154$–160 occurs around $t \approx 0.8$ s that corresponds to a similar increase of mass region $A = 161$–167, and a smaller increase of mass region $A = 168$–174, which results in a peak around $A \approx 165$. The nuclei populated at $t \approx 0.8$ s are important and shown as empty squares with a size proportional to their abundance. Part of these nuclei are included our measurements [see Fig. 5(c)]. The sensitivity study indicates that the half-lives of the nuclei far away from stability line with even neutron number are important in the beginning of the $(n,\gamma) \rightleftharpoons (\gamma,n)$ equilibrium, as they determine the initial abundance of progenitors. However, the nuclei in the measured region, which is closer to the stability line, provide a closer impact between odd and even neutron numbers [see Fig. 5(c)]. This is important to shape the final abundance of the REE peak through the competition between β decays and neutron captures.

A more quantitative estimate of the impact of newly measured β-decay half-lives on the shape of the REE peak is illustrated in Fig. 6, where the calculated r-process abundances using the new measurements are compared to calculations using theoretical half-lives from different models, respectively. The figure also shows the theoretical uncertainty estimated for each model, determined by varying theoretical half-lives within a factor of 2, which is an estimate of the uncertainty associated with theoretical models based on the comparison with experimental data for less exotic nuclei. From the figure it is clear that the new half-lives have a direct impact on the detailed shape of the REE peak. Changing the astrophysical conditions within reasonable ranges results in a different shape of the REE peak, but does not change the impact of half-lives on the calculated abundance. Above all, the new measurements remove a significant uncertainty in the calculations associated with theoretical half-lives. Alternatively, the sensitivities of rare-earth elemental abundance to our data as well as to the three theoretical models are much smaller, which could help to study the well-known characteristic referred to as r-process universality [38].

In summary, our experiment extends the limit of the known half-lives reaching for the first time into the region

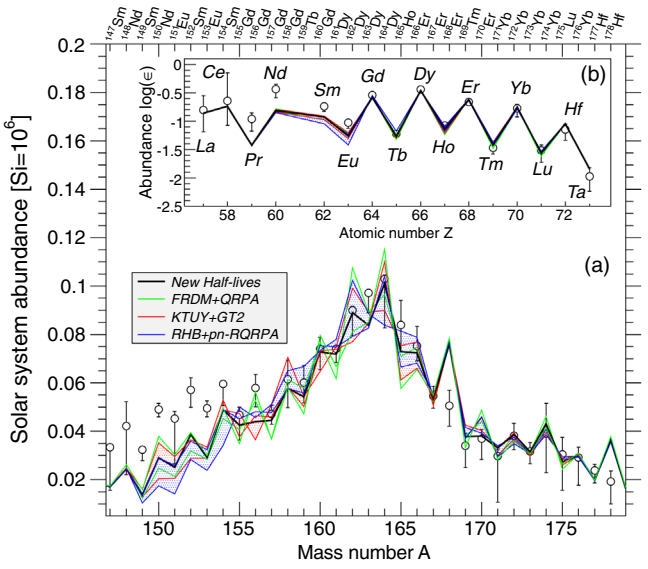

FIG. 6. (a) The *r*-process abundance pattern observed in the solar system (open circles) [39], and calculated using the experimental half-lives from this work (black line). The stable nuclei of each mass number are located on the top. The colored areas represent the uncertainty of calculated abundances, associated with half-life predictions of the models FRDM + QRPA (green), KTUY + GT2 (red), RHB + *pn*-RQRPA (blue). KTUY05 mass and ReaclibV1.0 database of nuclear reaction rates were employed for the baseline calculation. Experimental data and three theoretical predictions replaced the half-lives of nuclei whose values were measured for the first time. (b) Same as above but for the elemental abundance pattern compared with one metal-poor star HD108317 [40].

where the REE peak is expected to form based on some of the most promising *r*-process models [4,41]. Our data have a direct impact in *r*-process abundance calculations affecting almost all mass numbers between $A = 150$–170. This is an important step in the long-term goal of removing nuclear-physics uncertainties so that the REE peak can be used as a unique probe of the *r*-process freeze-out conditions and eventually reveal the currently unknown *r*-process site. Our data also allow the quantification of systematic problems of theoretical global models, and highlight the role of fine details of the β-decay strength functions in this exotic region of the nuclear chart. The comparison to theoretical models, however, does not show evidence of drastic changes of nuclear structure in the region of these measurements. This provides increased confidence in current mass models and, therefore, in the reliability of *r*-process calculations.

This work was carried out at the RIBF operated by RIKEN Nishina Center, RIKEN and CNS, University of Tokyo. The authors acknowledge discussion with Dr. Furong Xu, Dr. Haozhao Liang, and Dr. Kenichi Yoshida. We also acknowledge the EUROBALL Owners Committee for the loan of germanium detectors and the PreSpec Collaboration for the readout electronics of the cluster detectors. Part of the WAS3ABi was supported by the Rare Isotope Science Project which is funded by the Ministry of Education, Science, and Technology (MEST) and National Research Foundation (NRF) of Korea (2013M7A1A1075764). This work was partially supported by KAKENHI (Grants No. 25247045), the RIKEN Foreign Research Program, the Spanish Ministerio de Ciencia e Innovacin (Contracts No. FPA 2009-13377-C02 and No. FPA2011-29854-C04), the UK Science and Technology Facilities Council, the U.S. Department of Energy, Office of Science, Office of Nuclear Physics, Contract No. DE-AC02-06CH11357, under the auspices of the NNSA of the U.S. DOE at Los Alamos National Laboratory under Contract No. DE AC52-06NA25396, the NASA Grant No. NNX10AH78G, the National Research Foundation Grant funded by the Korean Government (Grants No. NRF-2009-0093817, No. NRF-2015R1D1A1A01056918, No. NRF-2016 R1A5A1013277, and No. NRF-2013R1A1A2063017), and the Hungarian Scientific Research Fund OTKA Contract No. K100835.

*wujin@ribf.riken.jp

[1] E. M. Burbidge, G. R. Burbidge, W. A. Fowler, and F. Hoyle, Rev. Mod. Phys. **29**, 547 (1957).
[2] M. Arnould, S. Goriely, and K. Takahashi, Phys. Rep. **450**, 97 (2007).
[3] G. J. Mathews and J. J. Cowan, Nature (London) **345**, 491 (1990).
[4] R. Surman, J. Engel, J. R. Bennett, and B. S. Meyer, Phys. Rev. Lett. **79**, 1809 (1997).
[5] M. R. Mumpower, G. C. McLaughlin, and R. Surman, Phys. Rev. C **86**, 035803 (2012).
[6] S. Goriely, J.-L. Sida, J.-F. Lemaître, S. Panebianco, N. Dubray, S. Hilaire, A. Bauswein, and H.-T. Janka, Phys. Rev. Lett. **111**, 242502 (2013).
[7] D. N. Schramm and W. A. Fowler, Nature (London) **231**, 103 (1971).
[8] Z. Patel *et al.*, Phys. Rev. Lett. **113**, 262502 (2014).
[9] M. R. Mumpower, G. C. McLaughlin, R. Surman, and A. W. Steiner, Astrophys. J. **833**, 282 (2016).
[10] S. Nishimura *et al.*, RIKEN Accel. Prog. Rep. **46**, 182 (2013).
[11] S. Nishimura *et al.*, Prog. Theor. Exp. Phys. **2012**, 03C006 (2012).
[12] P.-A. Söderström *et al.*, Nucl. Instrum. Methods Phys. Res., Sect. B **317**, 649 (2013).
[13] P.-A. Söderström *et al.*, AIP Conf. Proc. **1753**, 070001 (2016).
[14] J. Wu *et al.*, AIP Conf. Proc. **1594**, 388 (2014).
[15] E. Sahin *et al.*, Acta Phys. Pol. B **47**, 889 (2016).
[16] J. Wu *et al.*, EPJ Web Conf. **109**, 08003 (2016).
[17] G. Lorusso *et al.*, AIP Conf. Proc. **1594**, 370 (2014).
[18] P.-A. Söderström *et al.*, JPS Conf. Proc. **1**, 013046 (2014).
[19] N. Fukuda, T. Kubo, T. Ohnishi, N. Inabe, H. Takeda, D. Kameda, and H. Suzuki, Nucl. Instrum. Methods Phys. Res., Sect. B **317**, 323 (2013).
[20] Z. Y. Xu, PhD Thesis, University of Tokyo, 2011.

[21] S. Nishimura *et al.*, Phys. Rev. Lett. **106**, 052502 (2011).
[22] G. Lorusso *et al.*, Phys. Rev. Lett. **114**, 192501 (2015).
[23] Z. Y. Xu *et al.*, Phys. Rev. Lett. **113**, 032505 (2014).
[24] J. Wu *et al.*, JPS Conf. Proc. **6**, 030064 (2015).
[25] http://www.nndc.bnl.gov/.
[26] P. Möller, B. Pfeiffer, and K. L. Kratz, Phys. Rev. C **67**, 055802 (2003).
[27] H. Koura, T. Tachibana, M. Uno, and M. Yamada, Prog. Theor. Phys. **113**, 305 (2005).
[28] T. Tachibana, M. Yamada, and Y. Yoshida, Prog. Theor. Phys. **84**, 641 (1990).
[29] See Supplemental Material at http://link.aps.org/supplemental/10.1103/PhysRevLett.118.072701 for the table of 94 measured experimental half-lives.
[30] T. Marketin, L. Huther, and G. Martínez-Pinedo, Phys. Rev. C **93**, 025805 (2016).
[31] M. Wang *et al.*, Chin. Phys. C **36**, 1603 (2012).
[32] P. Möller, J. R. Nix, and K.-L. Kratz, At. Data Nucl. Data Tables **66**, 131 (1997).
[33] http://sourceforge.net/u/mbradle/blog.
[34] http://wwwndc.jaea.go.jp/nucldata/mass/KTUY04_E.html.
[35] S. Goriely, M. Samyn, and J. M. Pearson, Phys. Rev. C **75**, 064312 (2007).
[36] http://groups.nscl.msu.edu/jina/reaclib/db.
[37] M. Mumpower, J. Cass, G. Passucci, R. Surman, and A. Aprahamian, AIP Adv. **4**, 041009 (2014).
[38] K. Otsuki, G. J. Mathews, and T. Kajino, New Astron. **8**, 767 (2003).
[39] S. Goriely, Astro. Astrophys. **342**, 881 (2014).
[40] I. U. Roederer, J. E. Lawler, J. S. Sobeck, T. C. Beers, J. J. Cowan, A. Frebel, I. I. Ivans, H. Schatz, C. Sneden, and I. B. Thompson, Astrophys. J. Suppl. Ser. **203**, 27 (2012).
[41] M. R. Mumpower, G. C. McLaughlin, and R. Surman, Phys. Rev. C **85**, 045801 (2012).